



The cross-section shape-dependent responses of S and FOM of individual Au nanorod sensors

WanChun Yang¹ · YangXi Chen¹ · TianYi Fu¹ · Sheng Peng¹ · ChaoLing Du¹ · YuanGang Lu¹ · DaNing Shi¹

Received: 23 December 2018 / Accepted: 18 April 2019 / Published online: 22 April 2019
© Springer-Verlag GmbH Germany, part of Springer Nature 2019

Abstract

Besides aspect ratio (AR) and localized surface plasmon resonance (LSPR) peak wavelength, the cross-section shape of individual Au nanorod sensors is also crucial factors controlling their plasmon sensitivities. These three effects have not been investigated simultaneously till now. In this paper, we numerically investigate nanorods' cross-section-dependent responses both of refractive index sensitivity factor S and corresponding figure of merit FOM to their AR and LSPR peak wavelengths by discrete dipole approximation. The cross-section shapes are demonstrated to affect the values of S and FOM although it does not destroy the overall response tendency of S/FOM to LSPR peak wavelengths and AR . Their optimal LSPR spectral regions and AR are unveiled, which are revealed to be cross-section shape-dependent and independent, respectively. The triangular Au nanocolumn is revealed to provide good candidate for Au LSPR-based biological sensing and detection, whose optimal LSPR peak wavelength falls in the second near-infrared window.

1 Introduction

Individual nanoparticles, such as Au nanorods have found wide applications in surface-enhanced Raman scattering (SERS), optical sensing and detection, etc. [1–8]. This attributes to the resonant excitation of their localized surface plasmon resonances (LSPRs), known as the collective oscillating of free electrons of the rod responding to the incident light. Their optical spectra, including peak of the dipole LSPR and the corresponding peak width show wide tunability by their refractive indexes of surrounding mediums and the rod detailed geometries, such as cross-section shapes, and AR . This serves as the basement for their applications in LSPR-based refractive index sensing and detection, which depend on the excitation light wavelength and the rod detailed geometry. The parameters of refractive index sensitivity factor S [9] and figure of merit FOM [10] have been introduced to estimate their sensitivity performances, which are accessible

by their optical spectra, such as scattering spectra. Accordingly, to identify the optimal LSPR spectral region and AR for their plasmonic sensitivity applications of individual Au rod-like nanoparticles are significant, which may or may not be cross-section shape-dependent. Hence, it needs to be clarified. It is noted that investigations in literature [11–21] to optimize LSPR sensitivity either focus on to optimize the LSPR spectral region [15–18] or AR [19–21] separately and no reports devoted to simultaneously optimize LSPR spectral region and rod AR . To clarify the relationship between the optimized LSPR spectral region and AR is interesting accordingly. Additionally, the related reports mainly discuss S and/or FOM of non-rod nanoparticles, such as plate-like nanoparticles and nanowires [17, 21] while limited reports about nanorods and/or nanocylinders focus on nanorods with circular cross sections [19–21]. Yet, with fabrication technology development, other cross-section-shaped nanorods, may experimentally be met with, similar to semiconductor nanorods normally do [22, 23]. It is sorry that there are still no reports devoted to the optimized AR , neither optimized LSPR spectral region investigations for non-circular cross-section-shaped nanorods in literature to the best of knowledge. The different cross-section shapes are anticipated to affect both S and FOM response to AR and LSPR peak wavelengths of Au nanorod sensors as that of Au nanoplates [16]. Hence, different S , different optimal FOM , AR , and LSPR

Electronic supplementary material The online version of this article (<https://doi.org/10.1007/s00339-019-2654-1>) contains supplementary material, which is available to authorized users.

✉ ChaoLing Du
cldu@nuaa.edu.cn

¹ College of Science, Nanjing University
of Aeronautics and Astronautics, Nanjing 211100,
People's Republic of China

spectral region are expected, which needs to be clarified as well and is possibly cross-section shape dependent.

Accordingly, optical scattering spectra of individual Au rod-like nanosensors with different cross section (including triangle, square, pentagon, hexagon, and circular) shapes are numerically calculated by discrete dipole approximation (DDA) [24, 25] to investigate their cross-section-shape-dependent responses of S and FOM to LSPR peak wavelengths and AR simultaneously. It is revealed that under the same AR , the rod with triangle cross-section gets the largest S . Yet, regardless of their different cross-section shapes, their S is demonstrated to follow the same increasing trend with LSPR peak wavelengths. Meanwhile, their FOM is shown to get maximum $\sim 10 \text{ RIU}^{-1}$ at a broad optimal LSPR spectral region, which corresponds to an optimal AR region locating around 3.0 for all the concerned nanorods. These responses of S and FOM are analytically elucidated in terms of their dipole LSPR condition well.

2 Simulation structures and methods

Figure 1 schematically shows the structure diagram of the investigated different nanorods. For comparison, we have set the radius of the circumcircle of each rod being 10 nm in our simulations. The rod lengths are varied from ~ 20 to 100 nm to get different AR , which is defined as the ratio between rod lengths to their corresponding circumcircle diameters. The optical constants of Au are referred to the tabulated complex refractive indexes of Au in Ref. [26]. The scattering efficiency spectra of Au nanorods are then calculated by DDA on a cubic grid with a lattice constant equal to 1 nm, which unveil peak positions λ_{LSPR} of their dipole LSPR modes and the corresponding peak widths of full width at half maximum (FWHM). Then, S of their dipole LSPR mode is calculated, which has been defined as the derivative of λ_{LSPR} by n_m [9]. As shown in the supporting information,

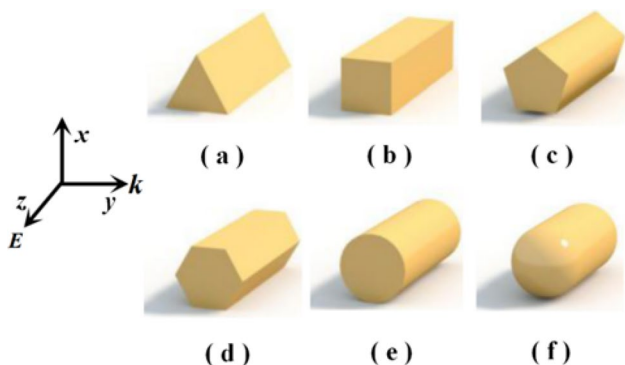


Fig. 1 The structure diagram of the investigated different nanorods, whose x - y cross sections being triangle (a), square (b), pentagon (c), hexagon (d), circle (e) and circle-2 (f), respectively

it is accessed by linear fitting of their corresponding λ_{LSPR} responding to n_m , the refractive index of the rods' surrounding medium. Starting from the data of S and FWHM, their FOM is then calculated, which refers to the ratio between their S to FWHM.

3 Results and discussions

Figure 2 shows that the scattering spectra of each concerned nanorods are sensitive to the refractive index n_m of their surrounding mediums, in which λ_{LSPR} red shifts from 1014/872/824/813/776/724 nm in water to 1142/981/922/908/865/803 nm in surrounding mediums with $n_m = 1.53$ for nanorods with triangle/square/pentagon/hexagon/circle/circle-2 cross section (perpendicular to the incident light polarization). Even at the same AR and n_m , their scattering spectra also differ, reflecting their different geometry, i.e., cross-section shape effects. The different λ_{LSPR} at the same AR and n_m also reveals that the smaller area of the rods' cross section, the larger red-shift of λ_{LSPR} compared to that of rod with circular cross section. These spectra characters originate from their n_m and cross-section shape-dependent electromagnetic field distributions while the inset of Fig. 2 and Fig. S1 of the supporting information show their typical electromagnetic near-field ($|E|$) distributions at their corresponding λ_{LSPR} as some examples by setting the amplitude of the electric field of the incident light to be unit.

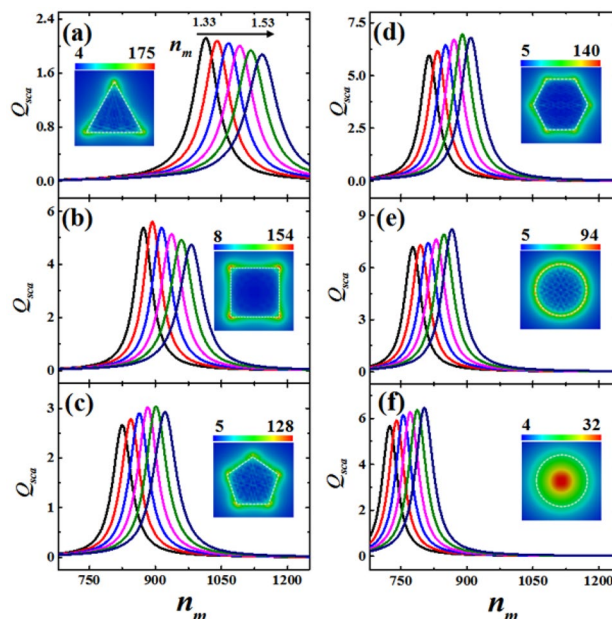


Fig. 2 The DDA calculated scattering efficiency spectra of the investigated Au nanorods under different n_m (linearly increasing from 1.33 to 1.53) with each AR being set to 3.0. The inset shows the near-field ($|E|$) distributions at their corresponding dipole λ_{LSPR} . a-f Corresponds to (a-f) Au nanorods in Fig. 1, respectively

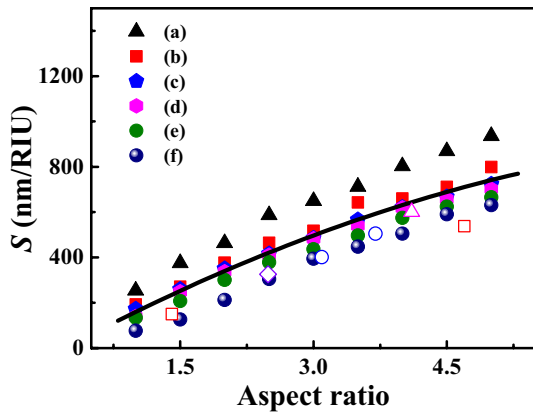


Fig. 3 The DDA calculated responses of S to AR of the investigated individual Au nanorods. The calculated data are noted to fall into an empirical quadratic prediction band of $S = -11.65AR^2 + 215.4AR - 44.39$ with maximum 59% prediction error. **a–f** Corresponds to **(a–f)** Au nanorods in Fig. 1, respectively. The data of hollow square, diamond, triangle, and circle refer to ref [14], [30], [31] and [32], respectively

Starting from the n_m -dependent spectra of Fig. 2, S of different nanorods are then calculated by linear fitting the data of their λ_{LSPR} versus n_m (see Fig. S2 of the supporting information). The obtained results are shown as Fig. 3, which are sensitive to rod’s AR . Figure 3 demonstrates that S increases steadily with AR for different nanorods with different cross-section shapes, confirming that AR is the key geometry parameter controlling S [21]. Yet, at the same AR , S of different rods are shown to be different, reflecting their different cross-section shape effect. For example, the rod with hemisphere capping and the rod with triangle cross section exhibit the smallest and largest S , respectively. This comes from their corresponding smallest and largest λ_{LSPR} at the same AR , which originates from their smallest and largest $|E|_{max}$ as demonstrated by the near-field $|E|$ distributions in the inset of Fig. 2. Moreover, it implies that Au nanorod with the less instead of more tips, hence smaller instead of larger areas of cross-sections, such as triangle rod, instead of pentagon and hexagon rods, gets larger $|E|_{max}$, then larger λ_{LSPR} and S . It is also noted that the increasing behavior of S with AR agrees with other available experimental data well [14, 30–32] as shown as hollow symbols in Fig. 3. Yet, experiments therein [14, 30–32] focuses on rods with circular cross sections while experimental data for rods with other cross sections, such as triangle cross sections are hence desired in the future. To further explore the surface (of the cross section of the rod perpendicular to the incident light polarization) area impact, S as a function of the surface area is plotted as Fig. S3 of the supporting information. It demonstrates that under the same AR , S increases with the surface area. Hence, smaller surface area is favoured to obtain higher S for LSPR-based nanosensors.

The responses of their S to λ_{LSPR} of Fig. 4 demonstrate that S increases with λ_{LSPR} from visible to near-infrared, which does not depend on their different geometries. Figure 4 also reveals that at the same λ_{LSPR} , S of different nanorods are approximate to each other. It indicates that the effect of rods’ cross sections (perpendicular to the incident polarization) on S responses to λ_{LSPR} is negligible. Accordingly, λ_{LSPR} provides the more general parameter governing S than that of AR while λ_{LSPR} is further determined by the detailed geometry of the nanorods, including AR and cross sections as demonstrated by Fig. 3. A closer check of Fig. 4 reveals that S increases with λ_{LSPR} linearly at visible region but increases with λ_{LSPR} non-linearly at near-infrared region. This agrees well with reports elsewhere [16] obtained from extinction spectra, which have been attributed to the optical response of the real part of Au dielectric constant $\epsilon_{rel}(Au)$ [16]. It applies to the results obtained from scattering spectra herein, too. As shown in the inset of Fig. 4, $\epsilon_{rel}(Au)$ responses to the incident light linearly $\epsilon_{rel1}(Au) = A' + B'\lambda$ and quadratically $\epsilon_{rel2}(Au) = A + B\lambda + C\lambda^2$ at visible and near-infrared regions (~760–1400 nm), respectively, with A, B, C, A' , and B' being fitting parameters. It contributes to the corresponding two different S expressions of the following Eqs. (1) and (2) of noble metal nanoparticles at visible and near-infrared regions, respectively.

$$S_1 = \frac{2}{n_m} \left(\lambda_{LSPR} + \frac{B'}{A'} \right), \tag{1}$$

$$S_2 = \frac{1}{n_m} \left[\left(\lambda_{LSPR} + \frac{B}{2A} \right) + \frac{\frac{C}{A} - \frac{B^2}{4A^2}}{\left(\lambda_{LSPR} + \frac{B}{2A} \right)} \right]. \tag{2}$$

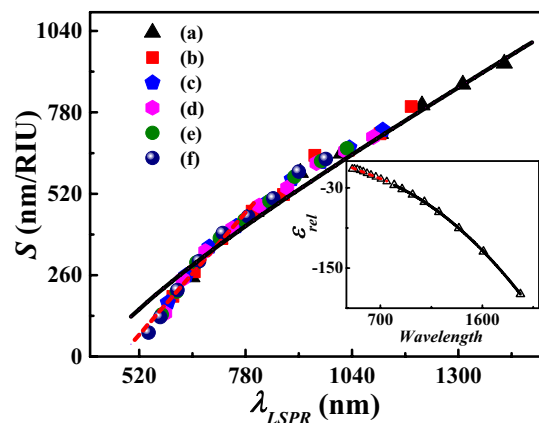


Fig. 4 The DDA calculated responses of S to the corresponding λ_{LSPR} of the investigated Au nanorods. **a–f** Corresponds to **(a–f)** Au nanorods in Fig. 1, respectively. The dashed and solid lines plotted the analytical results by Eqs. (1) and (2), respectively, while the inset dashed and solid line plotted the linear and nonlinear fitted $\epsilon_{rel}(Au)$ to the experimental $\epsilon_{rel}(Au)$ data [28]

These two equations are noted to agree with that of Ref. [15] and [27], respectively, which predicts S obtained from DDA calculated scattering spectra well at visible and near-infrared regions, respectively. The analytical results along with DDA calculated data indicate that to obtain high S , large excitation wavelength is preferred. Therefore, Figs. 3 and 4 demonstrate that among the concerned nanorods with the same AR , the rod with triangle cross section provides the best candidate for LSPR-based bio/chemical sensor, whose S is further able improved by increasing its λ_{LSPR} through increasing its AR .

Figure 5 presents the corresponding DDA-calculated FOM responses to the rod AR to identify their optimal AR , and then further to check the cross-section shape effect. Each set of the obtained FOM is shown to increase with AR initially till gets maximum, and then it decreases after surpassing their maximum, respectively. The optimal AR is revealed to be 3.0, 3.0, 2.5, 3.0, 3.0, 3.0, and 3.5 for the studied rod with triangle, square, pentagon, hexagon, circle, and circle-2 cross section, respectively, while the optimal AR for rod with circular cross-section (and with semi-sphere capping) matches well with available literate reports elsewhere [20, 27]. It is also noted that the optimal AR of all the concerned rods is approximate to each other, which all fall in $\sim 3.0 \pm 0.5$. This optimal AR region agrees with other available experimental report elsewhere [31, 32] as shown as hollow symbols in Fig. 5. Yet, experiments therein mainly focus on rods with circular cross sections while experimental data for non-circular cross-section rods are hence desired in the future. Figure 5 also reveals that the rods with triangle cross-section does not exhibit the largest FOM although it gets the largest S of all the rods. This attributes to the larger FWHM as revealed

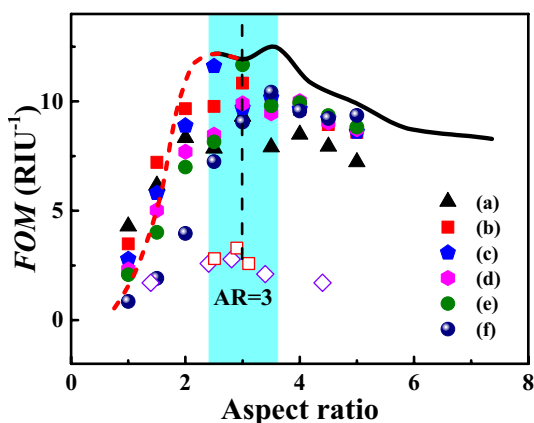


Fig. 5 The DDA calculated responses of FOM to AR of the investigated Au nanorods while the square labels the optimal AR region. **a–f** Corresponds to (**a–f**) Au nanorods in Fig. 1, respectively. The data of hollow Square and Diamond refer to ref [30] and [31], respectively. The dashed and solid lines present the analytical results at visible and near-infrared regions, respectively

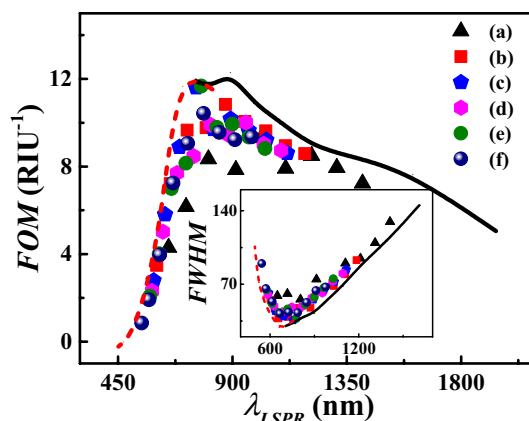


Fig. 6 The DDA calculated responses of FOM to the corresponding λ_{LSPR} of the investigated Au nanorods while the inset shows the DDA calculated responses of their corresponding FWHM to λ_{LSPR} . **a–f** Corresponds to (**a–f**) Au nanorods in Fig. 1, respectively. The dashed and solid lines present the analytical results at visible and near-infrared regions, respectively

in the inset of Fig. 6. However, its optimal FOM still fall in the same region $\sim 10 \pm 2$ RIU $^{-1}$ similar to the other rods. Hence, the cross-section shapes only have negligible effect on their optimal AR and FOM . Figure S4 of the supporting information shows the FOM responses of the concerned nanorods to the surface (of the cross section of the rod perpendicular to the incident light polarization) area at several typical AR . It reveals that at the same AR , the surface area impact on FOM of the nanorods is not obvious.

The obtained optimal AR and FOM are proposed to correspond to some specific λ_{LSPR} of the different rods, which provides significant information about the optimal LSPR spectral region, accordingly. The responses of FOM to λ_{LSPR} are plotted as Fig. 6, which shows that FOM initially increases with λ_{LSPR} for each the concerned rods regardless of their cross-section differences and then decreases with λ_{LSPR} increasing further after surpassing maximum. This is reasonable considering the variation of FWHM versus λ_{LSPR} and the increase of S with λ_{LSPR} . The inset of Fig. 6 shows that FWHM of the dipole LSPR mode initially decreases with λ_{LSPR} and gets minimum at ~ 700 nm, then it increases with λ_{LSPR} fast after surpassing the minimum FWHM. This variation and the increase of S with λ_{LSPR} as presented in Fig. 4 together contribute to the response of FOM of Fig. 6. Additionally, The maximum FOM is noted to locate at $\sim 1010/875/760/880/780/785$ nm for studied rod with triangle, square, pentagon, hexagon, circle, and circle-2 cross section, respectively, showing cross-section dependence. Their optimal FOM is noted to fall in the broad region $\sim 885 \pm 125$ nm. The large difference between the optimal λ_{LSPR} position for FOM is acceptable as the optimal AR for the concerned rods is approximate, which is approximate to each

other and contributes to the different λ_{LSPR} for the different cross-section-shaped rods. Hence, the different rod cross section leads to different surface scattering, further contributes to different λ_{LSPR} , hence different optimal λ_{LSPR} position for FOM . It is also noted that the LSPR peak wavelength of the optimal FOM is some larger than that of FWHM, which owns to the offset effect of the increasing behavior of S with λ_{LSPR} . The rod with triangle cross section is noted to get the smallest optimal FOM owing to its largest FWHM although it gets the largest S . Yet, its λ_{LSPR} is noted to fall in the second window of near-infrared. Hence, it is more favoured than the other concerned rods for biological applications as it still keeps high optimal $FOM \sim 10 \text{ RIU}^{-1}$.

Near λ_{LSPR} , FWHM of small noble metal nanoparticles (compared to the incident wavelength), including rods under investigation herein has been shown to follow [28].

$$FWHM = 2\epsilon_i|_{LSPR} / \left| \frac{d\epsilon_r}{d\lambda} \right|_{LSPR} \tag{3}$$

The analytical results by Eq. (3) have also been plotted in the inset of Fig. 6, which predicts nearly the same FWHM variation character, which gets minimum at $\sim 700 \text{ nm}$, in agreement with our DDA calculations. It comes from the negligible variation of $\frac{d\epsilon_r}{d\lambda}$ and the initial decrease till an minimum, then the increase with λ of ϵ_i . Then, FOM is analytically inferred to [10].

$$FOM = \frac{S}{FWHM} = \left| \frac{\epsilon_r}{n_m \epsilon_i} \right|_{LSPR} \tag{4}$$

by combining Eq. (3), S definition [9], and the dipole LSPR condition of $\epsilon_{rel}(Au) = -\kappa n_m^2$. Then, FOM is analytically inferred to be a function of λ_{LSPR} . Herein, κ is the shape factor of the concerned different nanorods, which is able to be calculated using spheroidal approximation. For all the concerned rods, they are proposed to be approximately taken as prolate nanoellipsoids, respectively. For each rods with non-circular cross section (perpendicular to the incident light polarization), its two axis are taken equal to the radius of the corresponding circumcircle of its above cross section while the rod length being the other axis. Then, κ is determined by $\kappa = (1 - L)/L$, which is further determined by AR of each the nanorods as presented below. The depolarization parameter along the incident polarization direction L is able to be given by the following Eq. (5) [29]. Herein, $e^2 = 1 - \frac{1}{AR^2}$ is the eccentricity of the nanoellipsoid.

$$L = \frac{1 - e^2}{e^2} \left(-1 + \frac{1}{2e} \ln \frac{1 + e}{1 - e} \right). \tag{5}$$

For nanorods with $AR < 8$ under investigated, Eq. (5) is simplified into [35].

$$L = (1 + AR)^{-1.6}. \tag{6}$$

The analytical results by Eq. (4) have also been plotted as lines in Fig. 6, which qualitatively capture the DDA calculated changing tendency of FOM for all the concerned different cross-section-shaped rods. It exhibits initial fast increase and gets maximum $\sim 12 \text{ RIU}^{-1}$ at optimal LSPR spectral region of $\sim 885 \pm 125 \text{ nm}$. The simple analytic results by Eq. (4) are independent of the detailed Au nanoparticle (nanorod herein) geometry, which relies only on Au dielectric response. It further contributes to the comparable optimal FOM at certain optimal LSPR spectral regions for all Au nanopartilce LSPR sensors regardless of their detailed geometries as obtained from DDA calculations. It also analytically explains why FOM gets maximum at certain AR for all the considered nanorods. This is owing to that the optimal λ_{LSPR} of each the nanorods just corresponds to their corresponding optimal κ , hence AR , respectively. Accordingly, FOM is directly a function of AR of each the concerned nanorods, which has been plotted as the solid and dashed lines in Fig. 5 at visible and near-infrared regions, respectively. It is demonstrated to capture the main characters of DDA-calculated response of Au nanorods' FOM to AR , which initially increases with AR and then decreases with increasing AR more after getting only a little higher maximum $FOM \sim 12 \text{ RIU}^{-1}$ than DDA at comparable optimal $AR \sim 3.0$ (labeled by the square) as that of DDA calculations. Therefore, as the analytical calculation of Eq. (4) is independent of the nanorod detailed geometries under the same circumcircle (hence the same AR), it accounts for the comparable predicted FOM for all the concerned nanorods under the same AR and also explains their approximate optimal FOM and optimal AR obtained from DDA calculations. Yet, the largest enhanced $|E|_{max}$ and $\sim 1010 \text{ nm}$ of λ_{LSPR} of the nanorod with triangle cross section is predicted to provide the best candidate among all the rods concerned for LSPR-based biological sensing and detection.

4 Conclusions

Our DDA calculations demonstrate that regardless of nanorods' different cross-section shapes, their S increases with λ_{LSPR} and AR steadily while the corresponding FOM shows a maximum responding to λ_{LSPR} and AR , respectively. Their cross-section shapes are also revealed to neither affect their optimal AR and optimal FOM , which locates at $\sim 3.0 \pm 0.5$ and $10 \pm 2 \text{ RIU}^{-1}$, respectively. This analytically attributes to Au optical responses and the fact that all the concerned nanorods fit for prolate nanoellipsoid approximation. However, their cross-section shapes are demonstrated to capable of reducing S value by increasing the sectional areas under the same AR . Meanwhile, the optimal LSPR spectral position for their optimal FOM is revealed to be cross-section shape dependent. The corresponding position

of Au triangular nanocolumn is shown to give the largest optimal LSPR peak wavelength ~ 1010 nm, which falls into the second near-infrared window, showing strong potential for future desirable applications in biological sensing and detection. The present work hold great promise for Au nanorod LSPR-based sensor designing and applications to access their optimal *AR*, spectral region, hence plasmon sensitivities with diverse possible cross-section shapes.

Acknowledgments This work was financially supported by the Fundamental Research Funds for the Central Universities (No. NS2016074), Natural Science Foundation of China (No. 11774171 and 11874220), and by Suzhou Applied Basic Research Program (No. SYG201546).

References

- Palash Bharadwaj, Pascal Anger, Lukas Novotny, *Nanotechnology* **18**, 044017 (2007)
- Sergei Kühn, Ulf Håkanson, Lavinia Rogobete, Vahid Sandogh-dar, *Phys. Rev. Lett.* **97**, 017402 (2006)
- F. Cannone, G. Chirico, A.R. Bizzarri, S. Cannistraro, *J. Phys. Chem. B* **110**, 16491 (2006)
- S.R. Anderson, M. Mohammadtaheri, D. Kumar, A.P. O'Mullane, M.R. Field, R. Ramanathan, V. Bansal, *Adv. Mater. Interface.* **3**, 1500632 (2016)
- S. Joshi, P. Pellacani, T.A. van Beek, H. Zuilhof, M.W.F. Nielen, *Sens. Actuators B Chem.* **209**, 505 (2015)
- Y.J. Jen, M. Suzuki, Y.H. Wang, M.J. Lin, *J. Appl. Phys.* **112**, 113111 (2016)
- W. Wang, Y. Peng, Z. Zhong, X. Tong, T. Liu, Y. Li, E. Ashalley, H. Chen, W. Jiang, Z. Wang, *Nanotechnology* **29**, 355402 (2018)
- S.L. Smitha, K.G. Gopchandran, T.R. Ravindran, V.S. Prasad, *Nanotechnology* **22**, 265705 (2011)
- H. Chen, X. Kou, Z. Yang, W. Ni, J. Wang, *Langmuir* **24**, 5233 (2008)
- L.J. Sherry, S.-H. Chang, G.C. Schatz, R.P. Van Duyne, B.J. Wiley, Y. Xia, *Nano Lett.* **5**, 2034 (2005)
- K.-S. Lee, M.A. El-Sayed, *J. Phys. Chem. B* **110**, 19220 (2006)
- E. Ringe, J.M. McMahon, K. Sohn, C. Cobley, Y. Xia, J. Huang, G.C. Schatz, L.D. Marks, R.P. Van Duyne, *J. Phys. Chem. C* **114**, 12511 (2010)
- B. Hazra, M. Chandra, *Acs Sens.* **1**, 536 (2016)
- J. Cao, T. Sun, K.T.V. Grattanab, *Sens. Actuators B Chem.* **195**, 332 (2014)
- M.M. Miller, A.A. Lazarides, *J. Phys. Chem. B* **109**, 21556 (2005)
- P. Sheng, C.L. Du, D.N. Shi, *Appl. Phys. A Mater. Sci. Proc.* **123**, 672 (2017)
- O. Saison-Francioso, G. Lévêque, R. Boukherroub, S. Szunerits, A. Akjouj, *J. Phys. Chem. C* **119**, 28551 (2016)
- M.A. Otte, B. Sepúlveda, W. Ni, J.P. Juste, L.M. Liz-Marzán, L.M. Lechuga, *Acs Nano* **4**, 349 (2010)
- Jan Becker, A. Trügler, A. Jakab, U. Hohenester, C. Sönnichsen, *Plasmonics* **5**, 161 (2010)
- J.S. Sekhon, S.S. Verma, *Plasmonics* **6**, 163 (2011)
- A.U. Khan, S. Zhao, G. Liu, *J. Phys. Chem. C* **120**, 19353 (2016)
- S. Peng, Y. Luo, P. Mao, C. Chen, J. Zhang, J. Tang, H. Lu, J. Yu, Z. Chen 15TH Int. Conf. Numer. Simul. Optoelectron. Devices Nusod **1** (2015)
- I. Iwantonno, S.K.M. Saad, R. Yuda, M.Y. Abd Rahman, A.A. Umar, *Superlattices Microstruct* **123**, 119–128 (2018)
- <http://www.ddscat.org>
- B.T. Draine, J. Goodman, *Astrophys. J.* **405**, 685 (1993)
- P.B. Johnson, R.W. Christy, *Phys. Rev. B* **6**, 4370 (1972)
- S. Peng, C.L. Du, D.N. Shi, *J. Light Scatt.* **30**, 77 (2018)
- W.C. Huang, J.T. Lue, *Quantum Phys. Rev. B* **49**, 17279 (1994)
- C.F. Bohren, D.R. Huffman, *Absorption and scattering of light by small particles* (Wiley, New York, 1983)
- H.J. Chen, L. Shao, K.C. Woo, Shape-dependent refractive index sensitivities of gold nanocrystals with the same plasmon resonance. *Phys. Chem. C* **113**, 17691 (2009)
- H.J. Chen, X.S. Kou, Z. Yang, Shape- and size-dependent refractive index sensitivity of gold nanoparticles. *Langmuir* **24**, 5233 (2008)
- J. Cao, M.H. Tu, T. Sun, Wavelength-based localized surface plasmon resonance optical fiber biosensor. *Sens. Actuators B* **181**, 611 (2013)

Publisher's Note Springer Nature remains neutral with regard to jurisdictional claims in published maps and institutional affiliations.